Supporting Information

$Ca_2La(MS_4)(BS_3)$ (M = Ge/Si and Sn/Si): Promising Infrared Nonlinear Optical Materials Designed by Atomic Site Co-occupancy Strategy

*Ya-Xiang Han, Chun-Li Hu, and Jiang-Gao Mao**

Section S1 Methods, Computational details, and References.

Synthesis

The start materials (with a purity higher than 99.9%), which were purchased from Beijing Hawk Science and Technology Co., Ltd., are BaS, CaS, La_2S_3, MO_2 (M = Ge and Sn), amorphous B powder, and S powder. They were used as received. The Si element comes from few added SiO_2 (One half of MO_2) or quartz tube.

Single crystals of $Ca_2La(MS_4)(BS_3)$ (M = Ge/Si and Sn/Si) were synthesized by a solid-state reaction under vacuum. In a glove box filled with argon gas, the BaS, CaS, La_2S_3, MO_2, amorphous B powder, and S powder with a molar ratio of 1:1:0.5:1:3:6 and a total weight of 0.3 g were loaded into a clean and open graphite crucible which is then put into a quartz tube. The quartz tubes were sealed with a hydrogen-oxygen flame under a high vacuum of 10^{-3} Pa. Next, the quartz tubes were placed into a computer-controlled muffle furnace, heated to 400 °C within 8 h and held for 24 h, then further heated to 900 °C (950 °C for $Ca_2La(Sn_{0.75}Si_{0.25}S_4)(BS_3)$) at a rate of 25 °C h^{-1}. After holding for 48 h, the system was cooled to 800 °C at 3°C h^{-1} and then cooled down to 600 °C at 1°C h^{-1}. Finally, the tubes were cooled to 400 °C at 5°C h^{-1} and turned the furnace off. Pale yellow or yellow crystals of $Ca_2La(Ge_{0.72}Si_{0.28}S_4)(BS_3)$ and $Ca_2La(Sn_{0.75}Si_{0.25}S_4)(BS_3)$ in about 70% yield with respect to Ca_2S were found after the quartz tubes were opened. The microcrystalline powder used for tests was obtained by grinding the $Ca_2La(MS_4)(BS_3)$ crystals sonicated with deionized water and ethanol, which proved the ability to resist moisture.

Single Crystal X-ray Diffraction

Single-crystal X-ray diffraction data for $Ca_2La(MS_4)(BS_3)$ (M = Ge/Si and Sn/Si) were collected at 293 K using an Agilent SuperNova dual-wavelength CCD diffractometer with Mo K_α radiation (λ = 0.71073Å). The CrysAlis Pro software package was utilized for data reduction. Numerical absorption corrections based on Gaussian integration over a multifaceted crystal model and empirical absorption corrections using spherical harmonics implemented in SCALE3 ABSPACK scaling algorithm were applied[S1]. The structures were determined by direct method and refined using full-matrix least-squares fitting on F^2 with SHELXL-2017[S2]. In the crystal structure models, Ca^{2+} and Ln^{3+} cations occupy the

same atomic site; Ge^{4+} (or Sn^{4+}) and Si^{4+} also occupy the same atomic site (CIF). PLATON[S3] was used for checking symmetry elements and no higher was given. Crystal date was shown in table S1.

Powder X-ray Diffraction

Powder x-ray diffraction data were collected via Rigaku MiniFlex600 diffractometer. Scanning was performed with a scan step width of 0.02° using Cu Kα radiation (λ = 1.541886 Å) in the 2θ range of 10 – 70°.

Energy-Dispersive X-ray Spectroscopy

Elemental analyses were carried out using a field-emission scanning electron microscope (JSM6700F) outfitted with an Oxford INCA energy-dispersive X-ray spectroscope.

Thermal Analysis

Thermogravimetric analysis (TGA) and differential thermal analysis(DTA) were performed with a NETZCH STA 449 F3 Jupiter® under a N_2 atmosphere, at a heating rate of 10℃/min.

Infrared Spectrum

IR spectra of $Ca_2La(MS_4)(BS_3)$ (M = Ge/Si and Sn/Si) were recorded on A Nicolet Magna 750 Fourier Transform Infrared spectrometer in the spectral range of 4000 to 400 cm^{-1}.

UV-Vis-NIR diffuse reflectance spectroscopy

The ultraviolet - visible - near-IR (UV-Vis-NIR) diffuse reflectance spectrum in the range of 200-2000nm was collected using a PerkinElmer Lambda 950 UV−vis−NIR spectrophotometer, with a barium sulfate powder plate as a 100% reflectance reference. Absorption data is converted from the reflection data by the Kubelka - Munk function $\alpha/S = (1 - R)^2/2R$ (α is the absorption coefficient, S the scattering coefficient, and R the reflectance. The band gap value is the abscissa of the intersection of the absorption edge extension line and the zero absorption.

Second-harmonic Generation

SHG response measurements were performed using the Kurtz and Perry method with a 2.05 μm Q-switched OPO Nd: YAG laser [S4]. Grind the crystals and sieve them into 6 particle sizes ranging from 45-53, 53-75, 75-105, 105-150, 150-210 and 210-300 μm, using microcrystalline $AgGaS_2$ with the same particle size range as a reference. The sample was placed on a glass microscope-covered slide, secured with a 1 mm thick silicone insole and a 5 mm diameter hole, and then covered with another glass slide. They were then placed into small tight boxes and probed under the pulsed infrared beam of a Q-switched Ho: Tm: Cr: YAG laser. The SHG signal was recorded on an oscilloscope connected to the detector. Standard IR NLO material of $AgGaS_2$ was used for all steps.

LIDT measurement

LIDT was measured using a 1 Hz 1064 nm Q-switch laser with $AgGaS_2$ as a reference. 150-210 μm particle size sample box was picked out for this test. For a point on the optical element (sample box), increasing pulse energy was raised from 1 mJ until the point is damaged.

Computational Method

The electronic structure and optical properties were analyzed by the plane wave pseudopotential method in the density functional theory (DFT) implemented in the total energy code CASTEP. [S5, S6] For the exchange and correlation functions, we chose Perdew-Burke-Ernzerhof (PBE) in the generalized Gradient Approximation (GGA) [S7]. The interactions between the ionic cores and the electrons were described by the norm-conserving pseudopotential [S8]. The following valence-electron configurations were considered in the computation: Ca $3s^2 3p^6 4s^2$, La $5d^1 6s^2$, B $2s^2 2p^1$, Ge $4s^2 4p^2$, Sn $5s^2 5p^2$ and S $3s^2 3p^4$. The numbers of plane waves included in the basis sets were determined by cutoff energies of 800 eV for all three compounds. Monkhorst-Pack k-point sampling of 3×1×4 was used to

perform numerical integration of the Brillouin zone. During the optical property calculations, approximately 288 empty bands were involved to ensure the convergence of linear optical properties and SHG coefficients for $Ca_2La(MS_4)(BS_3)$ (M = Ge/Si and Sn/Si) respectively. The calculations of second-order NLO properties were based on length-gauge formalism within the independent-particle approximation [S9]. We adopted Chen's static formula, which was derived by Rashkeev et al [S10]. and later improved by Chen's group [S11]. The static second-order NLO susceptibility can be expressed as

$$\chi^{\alpha\beta\gamma} = \chi^{\alpha\beta\gamma}(VE) + \chi^{\alpha\beta\gamma}(VH) + \chi^{\alpha\beta\gamma}(two\ bands)$$

where $\chi^{\alpha\beta\gamma}(VE)$ and $\chi^{\alpha\beta\gamma}(VH)$ give the contributions to $\chi^{\alpha\beta\gamma}$ from virtual-electron processes and virtual-hole processes, respectively, and $\chi^{\alpha\beta\gamma}(two\ bands)$ gives the contribution to $\chi^{\alpha\beta\gamma}$ from the two-band processes. The formulas for calculating $\chi^{\alpha\beta\gamma}(VE)$, $\chi^{\alpha\beta\gamma}(VH)$, $\chi^{\alpha\beta\gamma}(two\ bands)$ are given in ref S11.

References

(1) Blessing, R. H. An Empirical Correction for Absorption Anisotropy. Acta Crystallogr., Sect. A: Found. Crystallogr. **1995**, *51*, 33-38.

(3) Sheldrick, G. M. SHELXT - Integrated space-group and crystal-structure determination. Acta Crystallographica a-Foundation and Advances **2015**, *71*, 3-8.

(3) Spek, A. L. Single-crystal structure validation with the program PLATON. J. Appl. Crystallogr. **2003**, *36*, 7-13.

(4) S. K. Kutz, T. T. Perry, J. Appl. Phys. **1968**, *39*, 3798-3813.

(5) Milman, V.; Winkler, B.; White, J. A.; Pickard, C. J.; Payne, M. C.; Akhmatskaya, E. V.; Nobes, R. H. Int. J. Quantum Chem. **2000**, *77*, 895-910.

(6) Segall, M. D.; Lindan, P. J. D.; Probert, M. J.; Pickard, C. J.; Hasnip, P. J.; Clark, S. J.; Payne, M. C. J. Phys.: Condens. Matter **2002**, *14*, 2717-2744.

(7) Perdew, J. P.; Burke, K.; Ernzerhof, M. Phys. Rev. Lett. **1996**, *77*, 3865-3868.

(8) Lin, J. S.; Qteish, A.; Payne, M. C.; Heine, V. V. Phys. Rev. B: Condens. Matter Mater. Phys. **1993**, *47*, 4174-4180.

(9) Aversa, C.; Sipe, J. E. *Phys. Rev. B: Condens. Matter Mater. Phys.* **1995**, *52*, 14636-14645.

(10) Rashkeev, S. N.; Lambrecht, W. R. L.; Segall, B. *Phys. Rev. B: Condens. Matter Mater. Phys.* **1998**, *57*, 3905-3919.

(11) Lin, J.; Lee, M. H.; Liu, Z. P.; Chen, C. T.; Pickard, C. J. *Phys. Rev. B: Condens. Matter Mater. Phys.* **1999**, *60*, 13380-13389.

Table S1. Summary of Crystallographic data and structure refinements for $Ca_2La(MS_4)(BS_3)$ (M = Ge/Si and Sn/Si).

Formula	**$Ca_2La(Ge_{0.72}Si_{0.28}S_4)(BS_3)$**	**$Ca_2La(Sn_{0.75}Si_{0.25}S_4)(BS_3)$**
formula weight	518.88	564.63
temperature (K)	100(2)	150(2)
crystal system	Hexagonal	
space group	*P*6$_3$*mc* (No. 186)	
a (Å)	9.6433(2)	9.7146(9)
c (Å)	6.5320(2)	6.6425(7)
V (Å^3)	526.05(3)	542.89
Z	2	
ρ_{calc} (g/cm^3)	3.276	3.454
μ (mm^{-1})	8.562	8.353
F(000)	485	521
λ (Mo Kα) (Å)	0.71073	
R_{int}	0.0419	0.0601
Goodness-of-fit on F^2	1.106	1.120
R_1, wR_2 [I>2σ (I)][a]	0.0130, 0.0265	0.0220, 0.0420
R_1, wR_2 (all data)	0.0136, 0.0266	0.0281, 0.0459
flack parameter	-0.01(2)	-0.08(3)

[a]$R_1 = \Sigma||F_o|-|F_c||/\Sigma|F_o|$; and $wR_2 = \{\Sigma[w(F_o^2-F_c^2)^2]/\Sigma[w(F_o^2)^2]\}^{1/2}$.

Table S2. Atomic coordinates ($\times 10^4$) and equivalent isotropic displacement parameters ($Å^2 \times 10^3$) for $Ca_2La(MS_4)(BS_3)$ (M = Ge/Si and Sn/Si). U_{eq} is defined as 1/3 of the trace of the orthogonalised U_{ij} tensor.

Compounds	Atom	*x*	*y*	*z*	U(eq)
$Ca_2La(Ge_{0.72}Si_{0.28}S_4)(BS_3)$	Ca(1)	6197(1)	8098(1)	2082(1)	13(1)
	La(1)	6197(1)	8098(1)	2082(1)	13(1)
	Ge(1)	3333	6667	7803(1)	10(1)
	Si(1)	3333	6667	7803(1)	10(1)
	B(1)	10000	10000	841(9)	9(1)
	S(1)	915(1)	5457(1)	9108(1)	14(1)
	S(2)	3333	6667	4437(2)	11(1)
	S(3)	8906(1)	7812(1)	993(1)	10(1)
$Ca_2La(Sn_{0.75}Si_{0.25}S_4)(BS_3)$	Ca(1)	3789(1)	1894(1)	7908(1)	19(1)
	La(1)	3789(1)	1894(1)	7908(1)	19(1)
	Sn(1)	6667	3333	2266(1)	15(1)
	Si(1)	6667	3333	2266(1)	15(1)
	B(1)	0	0	9170(20)	15(3)
	S(1)	5411(1)	4589(1)	801(3)	23(1)
	S(2)	6667	3333	5744(6)	24(1)
	S(3)	1084(1)	-1084(1)	9041(3)	16(1)

Table S3. Selected bond distances (Å) for $Ca_2La(MS_4)(BS_3)$ (M = Ge/Si and Sn/Si).

Bond	**Length**	
	$Ca_2La(Ge_{0.72}Si_{0.28}S_4)(BS_3)$	**$Ca_2La(Sn_{0.75}Si_{0.25}S_4)(BS_3)$**
Ca(1)/La(1)-S(2)	2.8433(8)	2.816(2)
Ca(1)/La(1)-S(3)#1	2.8513(4)	2.8703(9)
Ca(1)/La(1)-S(3)	2.8513(4)	2.8704(9)
Ca(1)/La(1)-S(3)#2	2.8891(10)	2.908(2)
Ca(1)/La(1)-S(1)#3	2.9562(7)	2.9835(14)
Ca(1)/La(1)-S(1)#4	2.9562(7)	2.9835(14)
M(1)-S(2)	2.1989(15)	2.310(4)
M(1)-S(1)#8	2.1926(9)	2.326(2)
M(1)-S(1)#7	2.1926(9)	2.326(2)
M(1)-S(1)	2.1926(9)	2.326(2)
B(1)-S(3)#9	1.8301(8)	1.8265(17)
B(1)-S(3)#1	1.8302(8)	1.8265(17)
B(1)-S(3)	1.8301(8)	1.8265(17)

*M is defined as a combination of 0.72 Ge + 0.28 Si or 0.75 Sn + 0.25 Si.

Symmetry transformations used to generate equivalent atoms:

#1 -y, x-y, z; #2 x-y, x, z-1/2; #3 x, y, z+1; #4 -y+1, x-y, z+1; #5 -x+1, -y+1, z+1/2; #6 y, -x+y, z+1/2; #7 -x+y+1, -x+1, z; #8 -y+1, x-y, z; #9 -x+y, -x, z; #10 -x+y+1, -x+1, z-1; #11 x, y, z-1.

Table S4. Measured LIDTs of $Ca_2La(MS_4)(BS_3)$ (M = Ge/Si and Sn/Si).

Compounds	Spot area (cm^2)	Damage threshold (MW/cm^2)
$Ca_2La(Ge_{0.72}Si_{0.28}S_4)$ (BS_3)	0.02	26.36
$Ca_2La(Sn_{0.75}Si_{0.25}S_4)$ (BS_3)	0.02	25.36
AGS	0.02	4

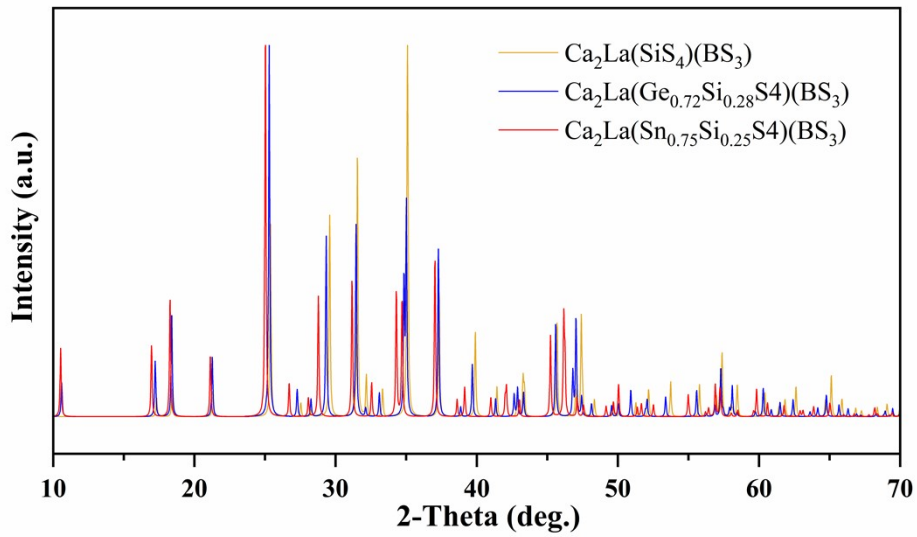

Figure S1. Overall PXRD peak shifts of $Ca_2La(Ge_{0.72}Si_{0.28}S_4)(BS_3)$ and $Ca_2La(Sn_{0.75}Si_{0.25}S_4)(BS_3)$.

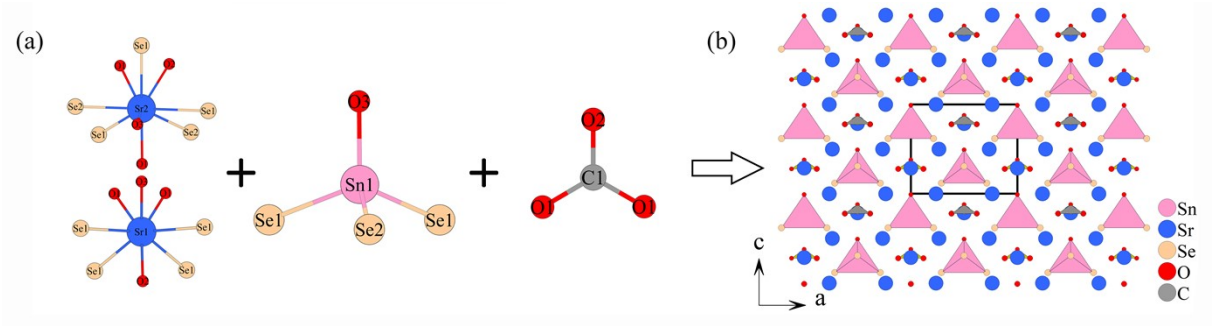

Figure S2. The SrO_4Se_4, SrO_4Se_5, $SnOSe_3$, CO_3 motifs in $Sr_3[SnOSe_3][CO_3]$ a); the integral crystal structure of $Sr_3[SnOSe_3][CO_3]$ viewed down the *b*-axis b).

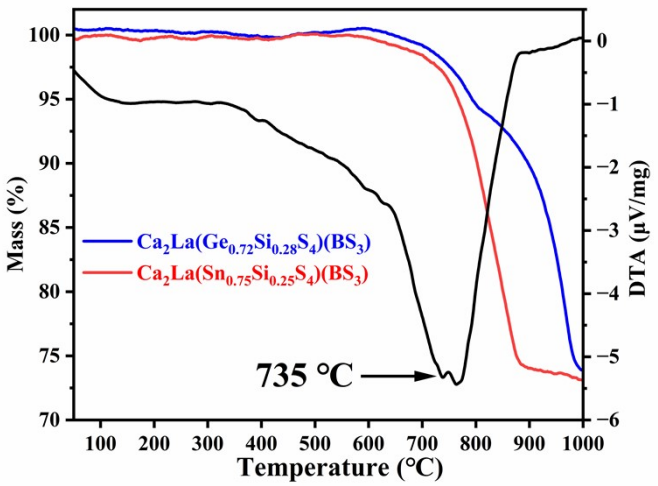

Figure S3. TGA and DTA curves for $Ca_2La(Ge_{0.72}Si_{0.28}S_4)(BS_3)$ and $Ca_2La(Sn_{0.75}Si_{0.25}S_4)(BS_3)$.

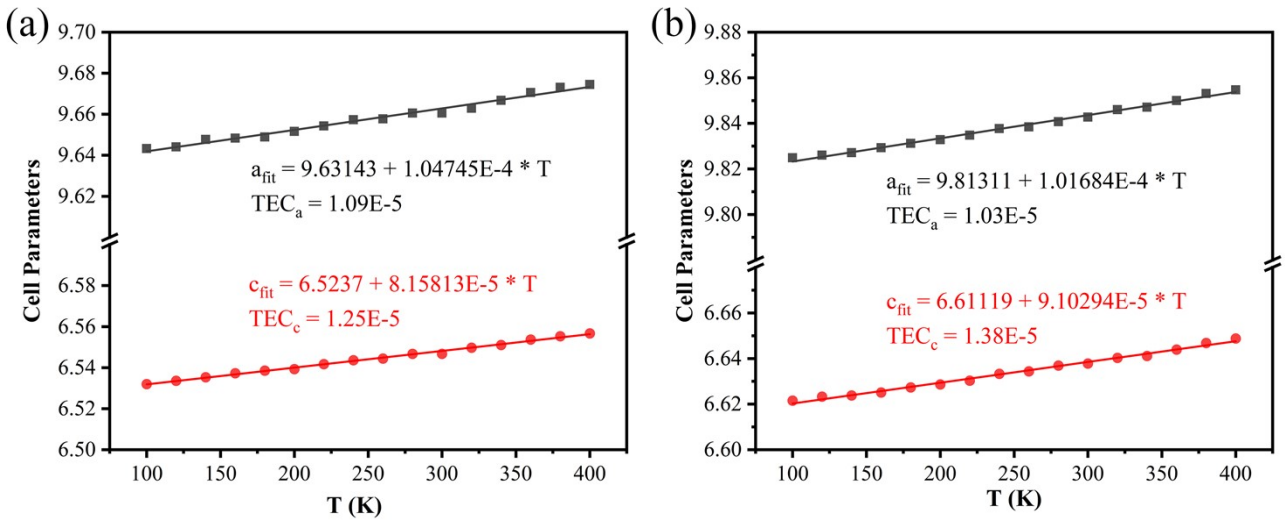

Figure S4. Linear fitting of cell parameters with temperature and the TECs of $Ca_2La(Ge_{0.72}Si_{0.28}S_4)(BS_3)$ (a) and $Ca_2La(Sn_{0.75}Si_{0.25}S_4)(BS_3)$ (b).

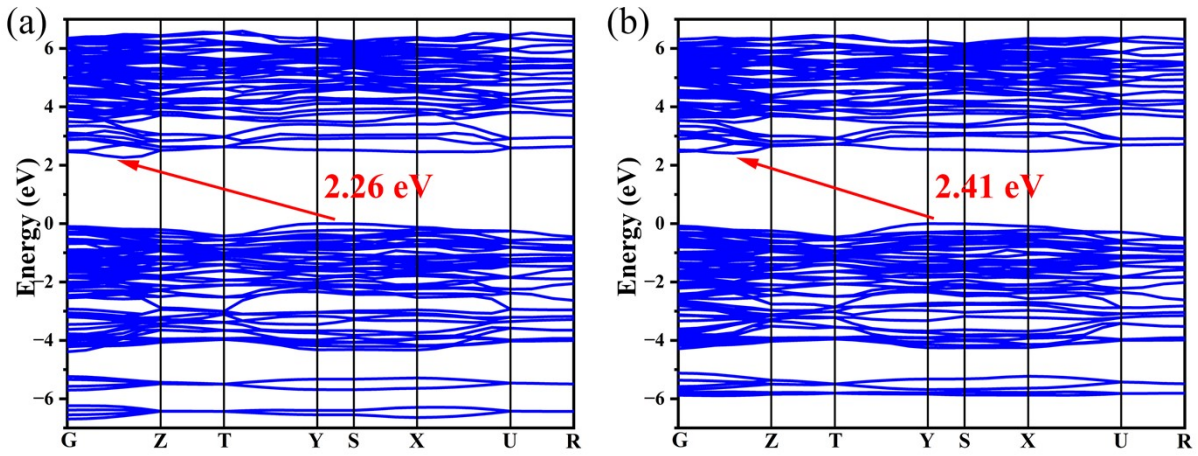

Figure S5. Calculated band structures of $Ca_2La(Ge_{0.72}Si_{0.28}S_4)(BS_3)$ (a) and $Ca_2La(Sn_{0.75}Si_{0.25}S_4)(BS_3)$ (b).

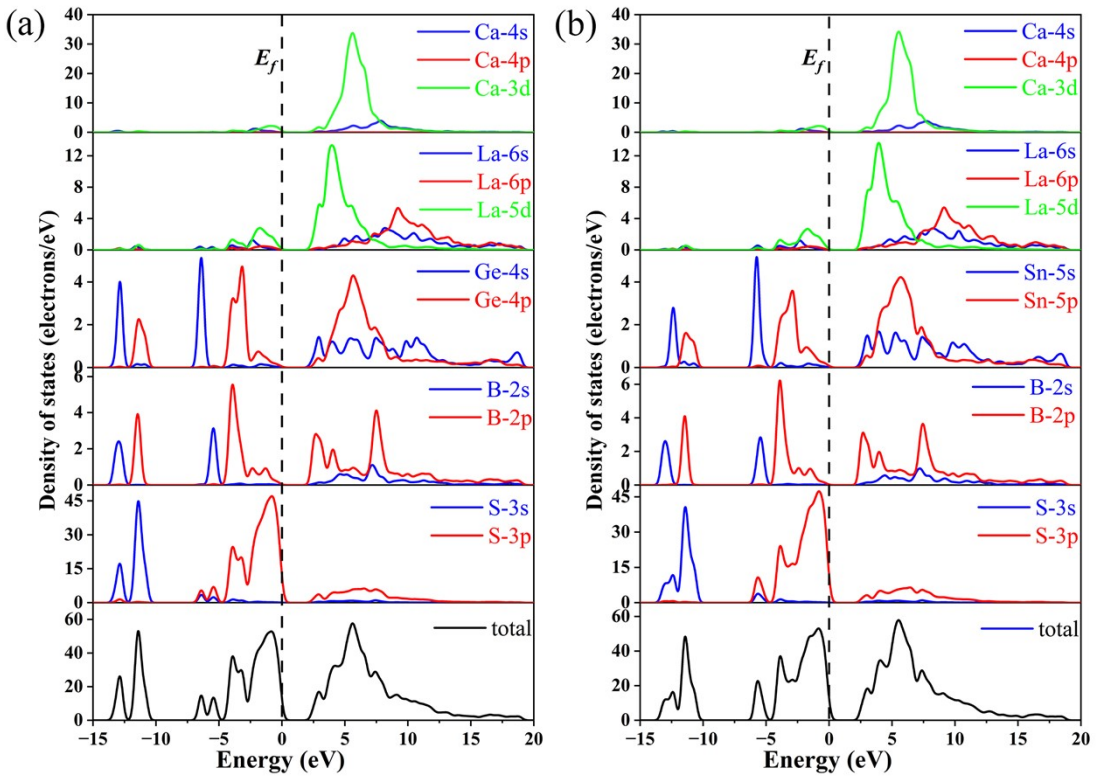

Figure S6. The density of states for $Ca_2La(Ge_{0.72}Si_{0.28}S_4)(BS_3)$ (a) and $Ca_2La(Sn_{0.75}Si_{0.25}S_4)(BS_3)$ (b).

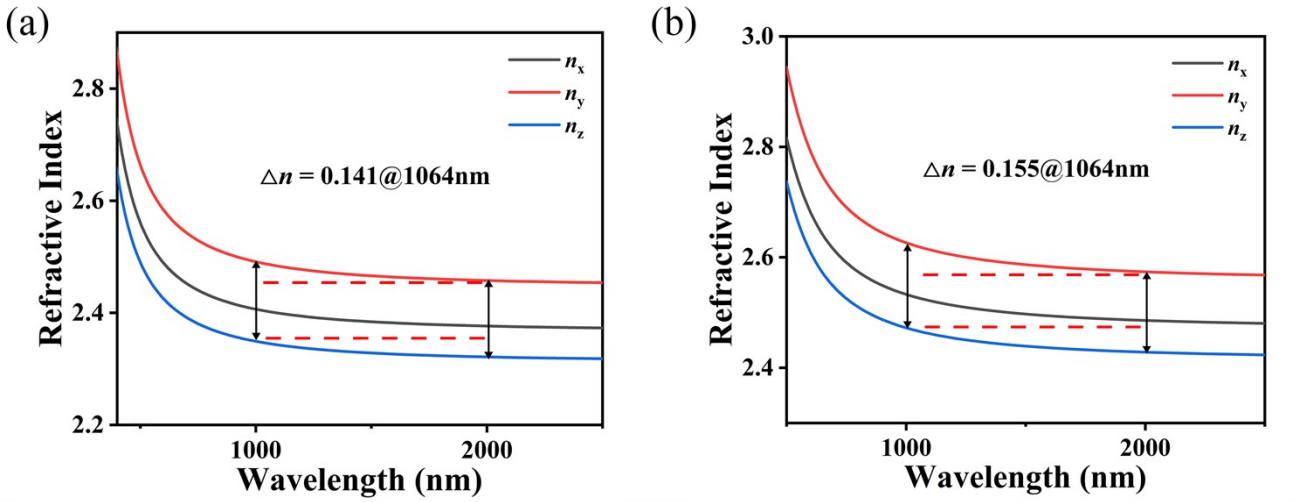

Figure S7. The calculated birefringence of $Ca_2La(Ge_{0.72}Si_{0.28}S_4)(BS_3)$ (a) and $Ca_2La(Sn_{0.75}Si_{0.25}S_4)(BS_3)$ (b).